Isocitrate dehydrogenase 1 mutations prime the all-trans retinoic acid myeloid differentiation pathway in acute myeloid leukemia

Héléna Boutzen,[1,2,3] Estelle Saland,[1,2] Clément Larrue,[1,2] Fabienne de Toni,[1,2] Lara Gales,[4,5,6] Florence A. Castelli,[7] Mathilde Cathebas,[1,2] Sonia Zaghdoudi,[1,2] Lucille Stuani,[1,2] Tony Kaoma,[8] Romain Riscal,[9,10,11] Guangli Yang,[12] Pierre Hirsch,[13,14,15,16] Marion David,[1,2] Véronique De Mas-Mansat,[1,2,3] Eric Delabesse,[1,2,3] Laurent Vallar,[8] François Delhommeau,[13,14,15,16] Isabelle Jouanin,[17,18] Ouathek Ouerfelli,[12] Laurent Le Cam,[9,10,11] Laetitia K. Linares,[9,10,11] Christophe Junot,[7] Jean-Charles Portais,[4,5,6] François Vergez,[1,2,3] Christian Récher,[1,2,3]* and Jean-Emmanuel Sarry[1,2]*

[1]Institut National de la Santé et de la Recherche Médicale (INSERM), Cancer Research Center of Toulouse, U1037, F-31024 Toulouse, France
[2]Université de Toulouse, F-31300 Toulouse, France
[3]Service d'Hématologie, Centre Hospitalier Universitaire de Toulouse, Institut Universitaire du Cancer Toulouse Oncopole, F-31059 Toulouse, France
[4]Université de Toulouse III Paul Sabatier, Institut National des Sciences Appliquées, UPS, Institut National Polytechnique, L'Ingénierie des Systèmes Biologiques et des Procédés, F-31077 Toulouse, France
[5]Institut National de la Recherche Agronomique (INRA), UMR792, Ingénierie des Systèmes Biologiques et des Procédés, F-31400 Toulouse, France
[6]Centre National de la Recherche Scientifique, UMR5504, F-31400 Toulouse, France
[7]CEA/DSV/iBiTec-S/SPI, Laboratoire d'Etude du Métabolisme des Médicaments, MetaboHUB-Paris, F-91191 Gif-sur-Yvette, France
[8]Genomics Research Unit, Centre de Recherche Public de la Santé, 1526 Luxembourg City, Luxembourg
[9]INSERM, U1194, Institut de Recherche en Cancérologie de Montpellier, F-34298 Montpellier, France
[10]Université de Montpellier and [11]Institut régional du Cancer Montpellier, F-34298 Montpellier, France
[12]Organic Synthesis Core Facility, Memorial Sloan-Kettering Cancer Center, New York, NY 10065
[13]Sorbonne Universités, Université Pierre-et-Marie-Curie (UPMC) Paris VI, UMR-S 938, CDR Saint-Antoine, F-75012 Paris, France
[14]INSERM, UMR-S938, CDR Saint-Antoine, F-75012 Paris, France
[15]Sorbonne Universités, UPMC Paris VI, GRC n°07, Groupe de Recherche Clinique sur les Myéloprolifératons Aiguës et Chroniques MyPAC, F-75012 Paris, France
[16]AP-HP, Hôpital Saint-Antoine, F-75012 Paris, France
[17]INRA, UMR1331, Toxalim, Research Centre in Food Toxicology, F-31027 Toulouse, France
[18]Université de Toulouse, INP, Toxalim, UMR1331, F-31027 Toulouse, France

Acute myeloid leukemia (AML) is characterized by the accumulation of malignant blasts with impaired differentiation programs caused by recurrent mutations, such as the isocitrate dehydrogenase (IDH) mutations found in 15% of AML patients. These mutations result in the production of the oncometabolite (R)-2-hydroxyglutarate (2-HG), leading to a hypermethylation phenotype that dysregulates hematopoietic differentiation. In this study, we identified mutant R132H IDH1-specific gene signatures regulated by key transcription factors, particularly CEBPα, involved in myeloid differentiation and retinoid responsiveness. We show that treatment with all-trans retinoic acid (ATRA) at clinically achievable doses markedly enhanced terminal granulocytic differentiation in AML cell lines, primary patient samples, and a xenograft mouse model carrying mutant IDH1. Moreover, treatment with a cell-permeable form of 2-HG sensitized wild-type IDH1 AML cells to ATRA-induced myeloid differentiation, whereas inhibition of 2-HG production significantly reduced ATRA effects in mutant IDH1 cells. ATRA treatment specifically decreased cell viability and induced apoptosis of mutant IDH1 blasts in vitro. ATRA also reduced tumor burden of mutant IDH1 AML cells xenografted in NOD–Scid–IL2rγ^{null} mice and markedly increased overall survival, revealing a potent antileukemic effect of ATRA in the presence of IDH1 mutation. This therapeutic strategy holds promise for this AML patient subgroup in future clinical studies.

*C. Récher and J.-E. Sarry contributed equally to this paper.

Correspondence to Jean-Emmanuel Sarry: jean-emmanuel.sarry@inserm.fr

Abbreviations used: 2-HG, 2-hydroxyglutarate; α-KG, α-ketoglutarate; AML, acute myeloid leukemia; APL, acute PML; ATRA, all-trans RA; BCL, B cell lymphoma; ChIP, chromatin immunoprecipitation; GSEA, gene set enrichment analysis; IDH, isocitrate dehydrogenase; L-CFU, leukemic CFU; LC/MS, liquid chromatography–mass spectrometry; NBT, nitrotetrazolium blue; PML, promyelocytic leukemia; qChIP, quantitative ChIP; qPCR, quantitative PCR; RA, retinoic acid; TF, transcription factor.

The Rockefeller University Press $30.00
J. Exp. Med. 2016 Vol. 213 No. 4 483–497
www.jem.org/cgi/doi/10.1084/jem.20150736

Despite progress in acute myeloid leukemia (AML) therapy, most patients relapse and die from the disease as a result of residual chemoresistant blasts. Thus, targeting this population is a mandatory requirement for effective AML therapy. In this context, mutations in isocitrate dehydrogenase 1 (IDH1) or IDH2 represent a promising therapeutic target. These mutations, originally identified in glioma (Dang et al., 2009), were then discovered in 15% of AML patients (Mardis et al., 2009) and have been found in an increasingly diverse set of other neoplasms, including hematological malignancies of both lymphoid and myeloid lineages (Lu et al., 2012; Fathi et al., 2014). Importantly, IDH mutations, which lead to the production of the oncometabolite (R)-2-hydroxyglutarate (2-HG), have been detected in preleukemic hematopoietic stem and multipotent progenitor cells as a persistent reservoir of surviving chemotherapeutic-resistant cells at remission (Shlush et al., 2014). Therefore, targeting IDH mutant cells might be essential to achieving long-term remission in the AML subgroup with IDH mutation.

An increasing number of studies have demonstrated that IDH1/2 mutations disrupt differentiation programs in nontransformed cells (Lu et al., 2012), as well as in hematopoietic and leukemic cells (Figueroa et al., 2010a; Sasaki et al., 2012; Losman et al., 2013). Moreover, tumors with IDH1/2 mutations exhibit a distinctive profile of 2-HG–dependent DNA and histone hypermethylation that alters gene expression (Figueroa et al., 2010a; Turcan et al., 2012), particularly for several genes involved in retinoic acid (RA) metabolism and signaling pathways (Chou et al., 2012; Guilhamon et al., 2013). Because RA is involved in granulocytic differentiation, we sought to specifically investigate the effects of all-trans-RA (ATRA) in the presence of the IDH1–R132H mutation in AML.

Our gene expression analyses demonstrate that IDH1–R132H mutation primes AML blasts to the granulomonocytic differentiation pathway compared with WT IDH1 AML cells and increases both H3K4me3 occupancy in the *CEPBα* gene promoter and expression of CEBPα, as well as downstream CEBPα target genes. Furthermore, we show a significant deregulation of RA-responsive target genes by IDH1–R132H mutation. Collectively, these observations suggest that 2-HG production resulting from IDH1 mutation biases hematopoietic differentiation toward the granulocytic lineage and further sensitizes mutant cells to ATRA-induced differentiation. Finally, we showed that the prodifferentiating effects of ATRA observed in the presence of IDH1 mutation at clinically achievable concentrations lead to a potent antileukemic response in AML cell lines and primary patient samples both in vitro and in vivo.

RESULTS AND DISCUSSION

As IDH mutations induce the production of neomorphic metabolite 2-HG, recent reports of 2-HG–dependent epigenetic programs (especially in genes involved in retinoid signaling pathways) are intriguing (Chou et al., 2012; Guilhamon et al., 2013). Seeking to determine whether AML cell lines engineered to express either the WT or mutant form of IDH1 (Fig. 1 A) and controlled for their production of 2-HG and α-ketoglutarate (α-KG; Fig. 1, B and C) have a specific gene signature, the gene expression profile of HL60 cells expressing the mutant IDH1–R132H was compared with WT cells by microarrays covering 23,924 human genes (Fig. 2). Computational analyses of these datasets identified two subsets of down- and up-regulated genes in mutant IDH1–R132H cells (Table S1) and their Gene Set Enrichment Analysis (GSEA) revealed significant enrichment of these signatures in published transcriptomes of 417 AML patients (cohort data available under Gene Expression Omnibus (GEO) accession no. GSE6891; Verhaak et al., 2009; Fig. S1, A and B), which validated our gene profiles specific to AML cells expressing mutant IDH1. Classification of biological processes down- or up-regulated by IDH1–R132H mutation particularly highlighted its role in immune responses, signaling pathways, metabolic processes, and cell differentiation (Table S1 and Fig. 2 A).

Furthermore, functional annotation of IDH1–R132H target genes revealed an enrichment of genes previously described as responsive to or regulated by several key transcription factors (TFs) essential for myelopoiesis, such as PU.1, RUNX1, GATA1, MECOM, MNDA, CEBPβ, and CEBPε (Table S2 and Fig. 2 B), and required for commitment to the monocytic and granulocytic lineages, such as CEBPα (Fig. 2 B). IDH1–R132H mutation also led to an increase in CEBPα expression at the RNA and protein level in both primary AML specimens (323 WT vs. 68 mutant IDH patients, respectively; GEO accession no. GSE6891; Verhaak et al., 2009; Fig. 2 C) and two AML cell lines (Fig. 2, C and D). As histone methylation is closely linked to mRNA expression and differentiation, especially in IDH mutant cells (Figueroa et al., 2010b; Kernytsky et al., 2015), we have shown that occupancy of the H3K4me3-activating locus in the *CEBPα* promoter was significantly increased in IDH1–R132H mutant HL60 and MOLM14 cells (Fig. 2 E). Because a peak of CEBPα expression occurred at the granulocyte-monocytic progenitor step of normal myelopoiesis (Radomska et al., 1998; Bagger et al., 2013; HemaExplorer database; Fig. S1 C), it is likely that IDH1–R132H mutation can drive AML blasts to this differentiation pathway through increased CEBPα expression. RT-PCR and immunophenotypical flow analyses indicated a significant increase in CEBPα-target genes RXRα, EMILIN, and CD11b (Laiosa et al., 2006; Hasemann et al., 2014) in the presence of mutant IDH1–R132H compared with WT IDH1 (Fig. 2, F–I). Quantitative chromatin immunoprecipitation (qChIP) experiments showed that mutant IDH1–R132H influences the recruitment of endogenous CEBPα to several of these target genes (Fig. 2 H). Moreover, IDH1–R132H mutation also modulated other myeloid differentiation-associated TFs (CEBPβ, PU.1, and RUNX1) and genes involved in the differentiation-related MAPK signaling pathway and associated metabolic processes (Fig. 2, A and B; Table S1 and S2), thus inducing a myeloid differentiation bias in these cells. Our results are consistent with

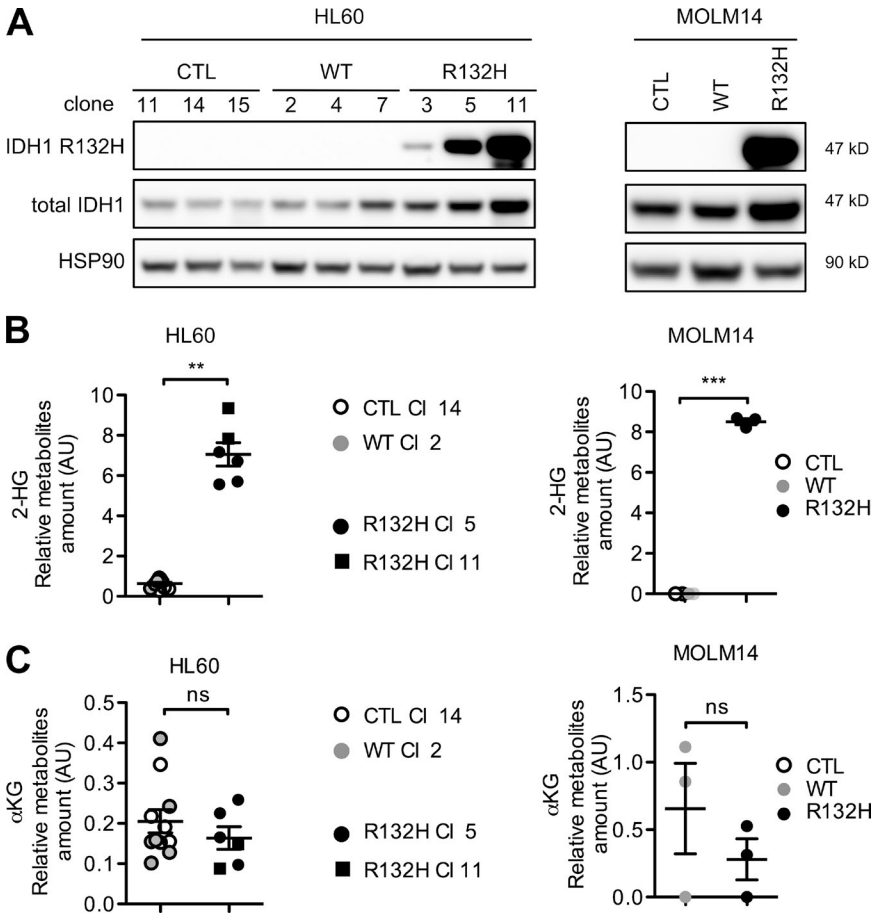

Figure 1. **AML cell lines engineered to express either WT IDH1 or mutant IDH1–R132H and producing the 2-HG oncometabolite.** (A) Western blot analysis of total and mutant form of IDH1 protein in diverse HL60 clones (left) or MOLM14 (right) infected with retroviruses encoding GFP alone (CTL) or GFP and the indicated IDH1 variants. One representative experiment of three experiments is shown. (B and C) LC-MS analysis of intracellular (R)-2-HG concentration (B) or intracellular α-KG concentration (C) in different clones of HL60 cell lines expressing either GFP control (CTL, clone 14), WT (clone 2), or mutant (R132H, clone 5 and 11) form of IDH1 in HL60 (left) or MOLM14 (right) cell lines. **, $P \leq 0.01$; ***, $P \leq 0.001$, statistical significance of the observed differences (Mann-Whitney test). $n = 5$ per condition.

recently published data demonstrating that IDH mutations favor differentiation toward the granulomonocytic lineage (Sasaki et al., 2012; Kats et al., 2014), while blocking erythroid differentiation (Losman et al., 2013; Wang et al., 2013a). It is noteworthy that the reintroduction of the CEBPα TF in hematopoietic stem/progenitor cells has the same effects as IDH1–R132H mutation in biasing differentiation toward the granulomonocytic lineage, while blocking the erythroid differentiation (Schepers et al., 2007). Finally, the overexpression of CEBPα sensitizes cells to differentiation into the granulocytic lineage with various agents (Ferrari-Amorotti et al., 2006).

Interestingly, gene expression analyses also revealed that the IDH1–R132H mutation gene signature is highly enriched in genes responsive to treatment with small molecules such as retinoids (e.g., ATRA or RA; Fig. 2 J), especially in promyelocytic leukemia (PML)/RA receptor α–driven acute promyelocytic leukemic (APL) cell lines and patients (Fig. S1 D) or, in some cases, of non-APL primary cells (Altucci et al., 2005). These observations corroborate a recently published metaanalysis showing a dysregulation of several genes involved in RA-related pathways in other cancers with IDH1–R132 (Guilhamon et al., 2013). Collectively, our gene expression analyses indicate that IDH1–R132H mutation can prime AML blasts toward granulomonocytic differentiation through the activation of the CEBPα pathway and could sensitize cells to ATRA-induced differentiation through the regulation of ATRA-responsive gene expression.

We tested this hypothesis using 25 primary AML patient specimens screened for their IDH1/2 mutational status in our cohort of 384 AML patients from Toulouse Hospital, which exhibit similar clinical features and distribution as those previously described in the literature (Abbas et al., 2010; Green et al., 2011; Table S3 and S4). We found that a clinically relevant concentration (1 μM) of ATRA induced the nuclear lobulation specifically associated with neutrophilic differentiation in eight primary AML patient samples harboring the IDH1–R132H mutation (Fig. 3 A) and producing 2-HG (Fig. 3 B). Moreover, treatment with ATRA was sufficient to increase the percentage of AML blasts expressing granulomonocytic differentiation markers (e.g., CD11b, CD15, and CD14) in 11 primary mutant IDH1–R132H AML samples (Fig. 3 C). Similar results were obtained for clinically ATRA-responsive APL samples used as a positive control (Fig. 3, A and C). In contrast, no increase in morphological changes and the CD14 marker, and only very modest decrease or increase in CD11b and CD15, respectively, were observed at any time point after ATRA treatment of primary AML blasts expressing WT IDH1 (Fig. 3, A and C). Consistent with data in primary

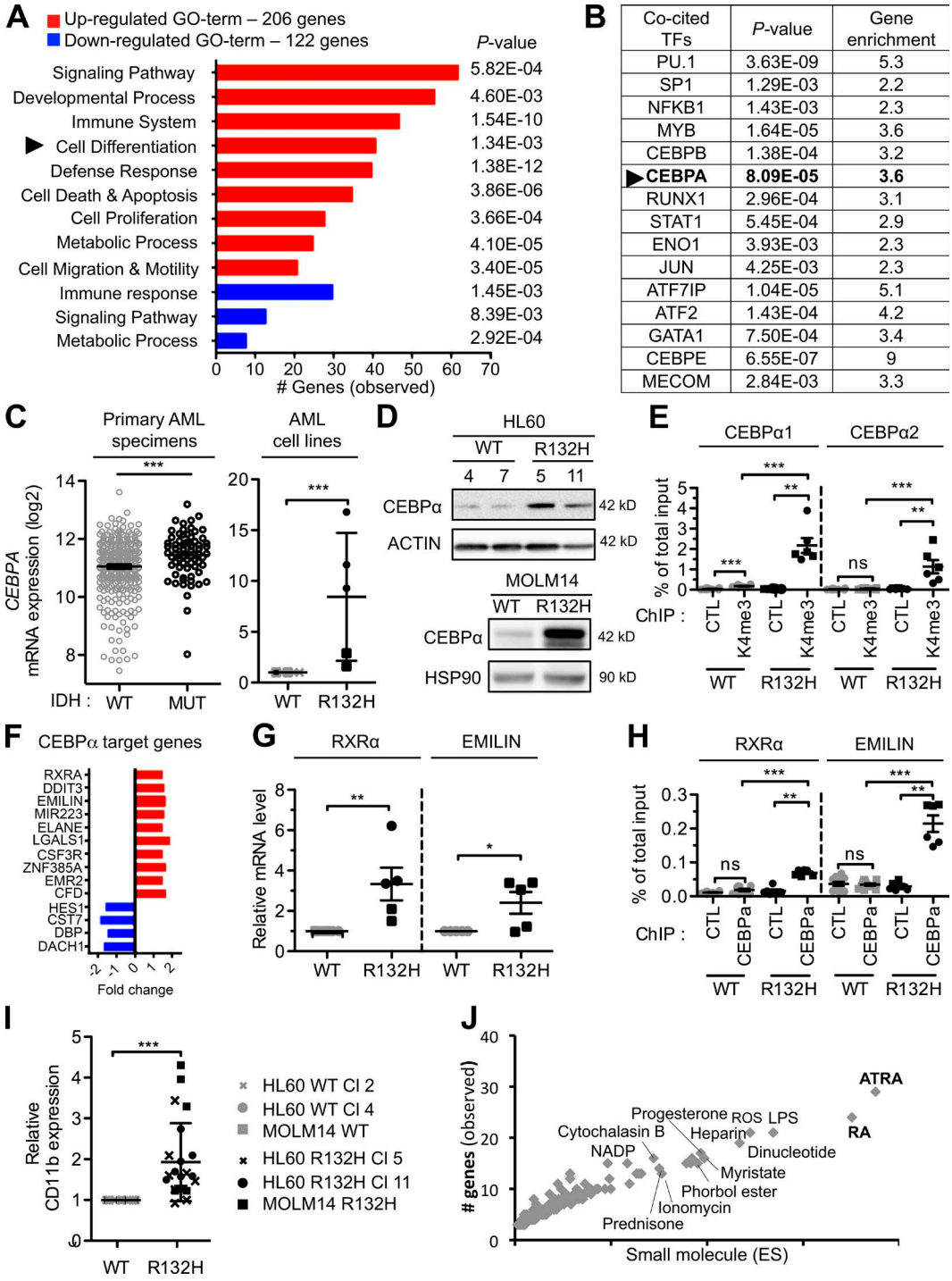

Co-cited TFs	*P*-value	Gene enrichment
PU.1	3.63E-09	5.3
SP1	1.29E-03	2.2
NFKB1	1.43E-03	2.3
MYB	1.64E-05	3.6
CEBPB	1.38E-04	3.2
▶**CEBPA**	**8.09E-05**	**3.6**
RUNX1	2.96E-04	3.1
STAT1	5.45E-04	2.9
ENO1	3.93E-03	2.3
JUN	4.25E-03	2.3
ATF7IP	1.04E-05	5.1
ATF2	1.43E-04	4.2
GATA1	7.50E-04	3.4
CEBPE	6.55E-07	9
MECOM	2.84E-03	3.3

Figure 2. **IDH1 mutation primes AML cells to the ATRA differentiation pathway through the activation of granulomonocytic differentiation–associated genes.** (A) Gene ontology enrichment analysis of down- (122) and up-regulated (206) genes from RNA expression profile of the differentially expressed genes between WT IDH1 HL60 clones and mutant IDH1–R132H HL60 clones by 1.5-fold or more ($n = 3$ clones for each cell type). (B) Gene to TF associations within mutant IDH1–R132H target genes using data mining algorithm (Genomatix). (C) mRNA expression of C/EBPα in WT (gray; $n = 323$) or mutant (black; $n = 68$) primary AML patients from the AML patient cohort GSE6891 (Verhaak et al., 2009) and in WT (gray) or R132H (black) HL60 (dots) or MOLM14 (square). (D) Protein level of CEBPα in mutant IDH1 HL60 (R132H, clone 5 and 11) and MOLM14 (R132H) cells or of WT IDH1 HL60 (WT, clone 4 and 7) and MOLM14 (WT) cells by Western blot ($n = 3$). (E) qChIP experiments showing the relative recruitment of histone H3 trimethylation at lysine 4 (H3K4me3) on CEBPa promoter in mutant IDH1–R132H HL60 and MOLM14 cells versus WT IDH1–WT HL60 and MOLM14 cells, as indicated. The precipitated DNA fragments were subjected to real-time PCR analysis with two different pairs of primers amplifying the CEBPα promoter. Results were represented as

AML cells, we observed significantly higher ATRA-induced increase of the CD11b myeloid differentiation marker in two cell lines with the IDH1–R132H mutation (Fig. 4 C). These results were reproduced in two independent clones of each category (CTL, IDH1–WT, and IDH1–R132H; Fig. 4 B) in a dose-dependent manner (Fig. 4 C). Consistent with well-described works in the literature (Radomska et al., 1998; Altucci et al., 2005), our control and WT IDH1 AML cell lines respond to ATRA but at a much lower level than IDH1–R132H AML cell lines (Fig. 4, A–C). ATRA also triggered granulocytic differentiation of mutant IDH1–R132H cells, as indicated by increased granulocytic enzyme activity measured with the nitrotetrazolium blue (NBT) reduction assay after 12 d (Fig. 4 D). Furthermore, gene expression profiling identified a 2-HG– and mutant IDH1–specific subset of 61 and 104 ATRA differentially expressed genes, respectively (Fig. 4 E). This gene signature is enriched in several TFs (e.g., RUNX1, PU.1, and CEBPε) modulating myeloid differentiation genes (e.g., IER3, PRAM1, and vimentin) and TFs (e.g., IRF1/7, STAT1, and PML) linked to IFN signaling (Table S5). Interestingly, ATRA-induced genes under PU.1 or CEBPε do not fully overlap with those induced by IDH1–R132H mutation (Fig. 4 E vs. Table S2), and IFN-stimulated genes are activated by RA (Chelbi-Alix and Pelicano, 1999; Shen et al., 2011), suggesting that cross talk may occur between these two distinct transcriptional programs.

Because ATRA-induced CD11b expression correlates with the expression of IDH1–R132H protein and with the level of 2-HG production (Fig. 4, A–C compared with Fig. 1, A and B), we asked whether exogenous 2-HG would sensitize AML cells to ATRA-induced differentiation. Pretreatment with a cell-permeable form of 2-HG (1-octyl-[R]-2-HG) increased the intracellular 2-HG concentration (Fig. 4 F) and sensitized NB4, HL60, and MOLM14 cells to ATRA-induced differentiation (Fig. 4 G). In contrast, the inhibition of IDH1–R132H activity using a mutant IDH1–specific inhibitor AGI-5198 significantly reduced both the production of 2-HG (Fig. 4 H) and the sensitivity of mutant IDH1–R132H cells to ATRA (Fig. 4 I). This confirms that 2-HG production is, at least in part, responsible for the enhanced sensitivity of IDH1–R132H expressing cells to ATRA-induced differentiation.

We also tested whether ATRA-induced terminal differentiation would preferentially lead to the reduction of cell proliferation and to cell death of mutant IDH1–R132H AML cells in vitro. As expected, 10-d treatment with ATRA induced a significant decrease in cell viability (Fig. 5 A) in mutant IDH1–R132H cells without affecting WT or control IDH1 cells. Moreover, ATRA treatment induced a mutant IDH1–specific apoptotic cell death, as shown by the increase of the Annexin V marker (Fig. 5, B and C) and cleavage of poly (ADP-ribose) polymerase and caspase-3, specifically in mutant IDH1–R132H AML cells (Fig. 5 D). This correlated with a marked decrease of antiapoptotic B cell lymphoma 2 (BCL2) protein (Fig. 5 D) in mutant IDH1–R132H cells. It is notable that it has been recently demonstrated that mutant IDH1/2 AML cells exhibited BCL2 dependency (Chan et al., 2015). Altogether, the reduction of cell viability and the induction of apoptosis led to a specific and marked reduction in the size and number of L-CFUs after ATRA treatment (Fig. 5, E and F).

To evaluate the ability of ATRA treatment to induce myeloid differentiation in vivo, we used a xenograft model based on immunodeficient NOD–scid IL2rγ^{null} (NSG) mice with primary AML samples or MOLM14 carrying the IDH1–R132H mutation (Fig. 6, A and G, respectively). We initiated ATRA treatment when the disease was well established and showed that ATRA specifically differentiated mutant IDH1–R132H cells xenografted in NSG mice, as indicated by morphological changes (Fig. 6, B and C) and an increase of CD11b^{+} myeloid cells in three primary AML patient samples (Fig. 6 D, bone marrow; Fig. 6 E, spleen; Fig. 6 F, peripheral blood) or MOLM14 cell line (Fig. 6 H). Furthermore, ATRA significantly reduced bone marrow tumor burden in a dose-dependent manner (Fig. 6 I) and led to a significant increase in overall survival of mice (Fig. 6 J). In contrast, we did not observe either prodifferentiative or antileukemic effects of ATRA in the WT IDH1 MOLM14 xenograft model (Fig. 6, K–M). Collectively, these data demonstrated that ATRA specifically induces differentiation and reduces tumor growth in the mutant IDH1–R132H subgroup of AML both in vitro and in vivo.

In summary, IDH1 mutation and its (R)-2-HG dysregulate downstream target pathways of myeloid-specific TFs, especially CEBPα, priming mutant IDH1–R132H AML blasts to the granulomonocytic lineage. Moreover, ATRA treatment down-regulates the expression of the protoonco-

the relative ratio between the mean value of immunoprecipitated chromatin with the indicated antibodies and the one obtained with a control irrelevant antibody. ChIP values are presented as percentage of total input. Data represent the mean of three independent experiments. Error bars represent SEM. (F) Among TFs identified in this study, up- (red) or down-regulation (blue) of CEBPα downstream target genes in mutant IDH1–R132H HL60 cells compared with WT IDH1 HL60 cells. (G) Expression of two CEBPα-target genes (RXRα and EMILIN) were analyzed in mutant IDH1 HL60 (R132H, clone 5 and 11) and MOLM14 (R132H) cells or in WT IDH1 HL60 (WT, clone 4 and 7) and MOLM14 (WT) cells by RT-qPCR. (H) qChIP experiments showing the relative recruitment of CEBPα on the RXRa or EMILIN locus in mutant IDH1–R132H HL60 and MOLM14 cells versus WT IDH1–WT HL60 and MOLM14 cells, as indicated. Results were presented as the relative ratio between the mean value of immunoprecipitated chromatin with the indicated antibodies and the one obtained with a control irrelevant antibody. Data represent the mean of three independent experiments. Error bars represent SEM. (I) Expression of the myeloid differentiation marker CD11b in HL60 and MOLM14 expressing mutant IDH1–R132H (clone 5 or 11) or WT IDH1 protein were assessed by flow cytometry (mean ± SD; $n = 6$). (J) Genes to small molecule associations within mutant IDH1–R132H target genes using data mining algorithm (genomatix). *, $P \leq 0.05$; **, $P \leq 0.01$; and ***, $P \leq 0.001$ indicate statistical significance of the observed differences (Mann-Whitney test).

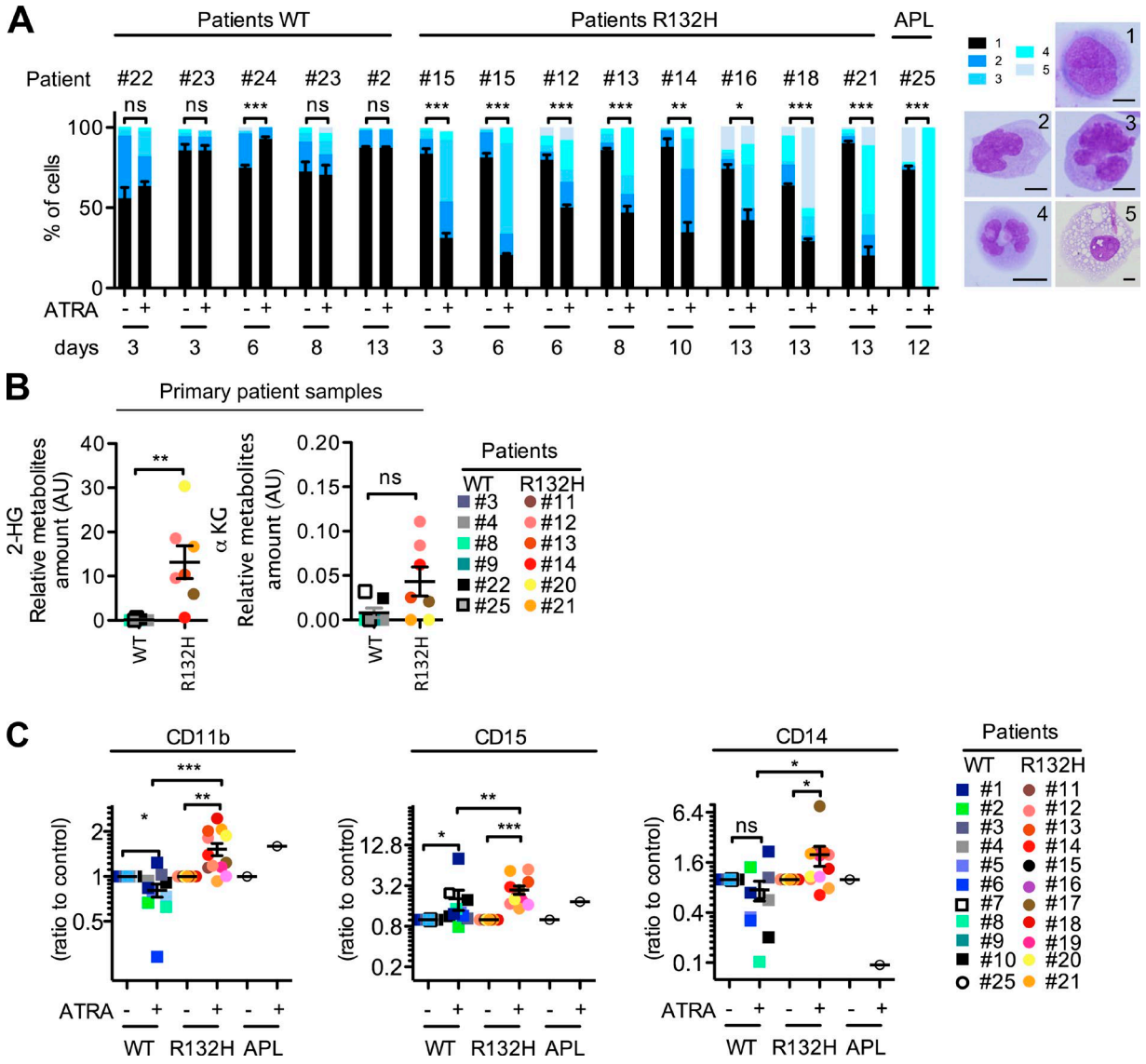

Figure 3. **IDH1–R132H mutation sensitizes to ATRA-induced differentiation of primary patient samples in vitro.** (A–C) ATRA treatment induces granulocytic differentiation of 11 primary patient samples carrying mutant IDH1–R132H (R132) compared with 10 WT IDH1 (WT) and 1 PML-RARα fusion protein (APL). (A) Primary WT IDH1, mutant IDH1–R132H AML, or APL patient samples were treated with ATRA at 1 µM for the indicated time, cytospun, and stained with May-Grünwald Giemsa. Cells were classified in five categories (from less to more differentiated; right). Bar, 10 µm. 100 cells per condition were counted three times for statistical analysis (Mann-Whitney test). (B) Intracellular amounts of 2-HG and α-KG in 12 primary patient samples expressing WT IDH1 (WT) or mutant IDH1–R132H (R132H), determined by Liquid chromatography–mass spectrometry (LC/MS; method 2). The amounts were normalized using a labeled standard, [^{13}C]-succinate, spiked with the same volume in each sample (y axis). A $\log_{10}$ scale was used. **, $P < 0.05$; Mann-Whitney test. (C) Flow cytometry analysis of CD11b, CD15, and CD14 expression was performed in primary WT IDH1, mutant IDH1–R132H AML, or APL patient samples treated with 1 µM ATRA or vehicle for 12 d (mean ± SEM). *, $P \leq 0.05$; **, $P \leq 0.01$; and ***, $P \leq 0.001$ indicate statistical significance of the observed differences (Wilcoxon matched pairs signed rank test).

genic protein BCL2, followed by the reduction of cell viability through the induction of apoptotic cell death in vitro. ATRA also has an in vivo antileukemic effect, specifically in mutant IDH1–R132H AML cells. These data suggest that IDH1–R132H mutation could be a valuable biomarker to select AML patients for ATRA treatment. Results from clinical trials with ATRA have been conflicting (Schlenk et al., 2009; Burnett et al., 2010; Nazha et al., 2013), but because IDH1 mutational status of those patients was not monitored in these studies, it would also be enlightening to reanalyze results of clinical trials conducted in non-APL patients to address the impact of IDH mutations on ATRA therapy. Interestingly, high serum 2-HG levels represented a negative prognostic factor independent of other clinical and molecular features

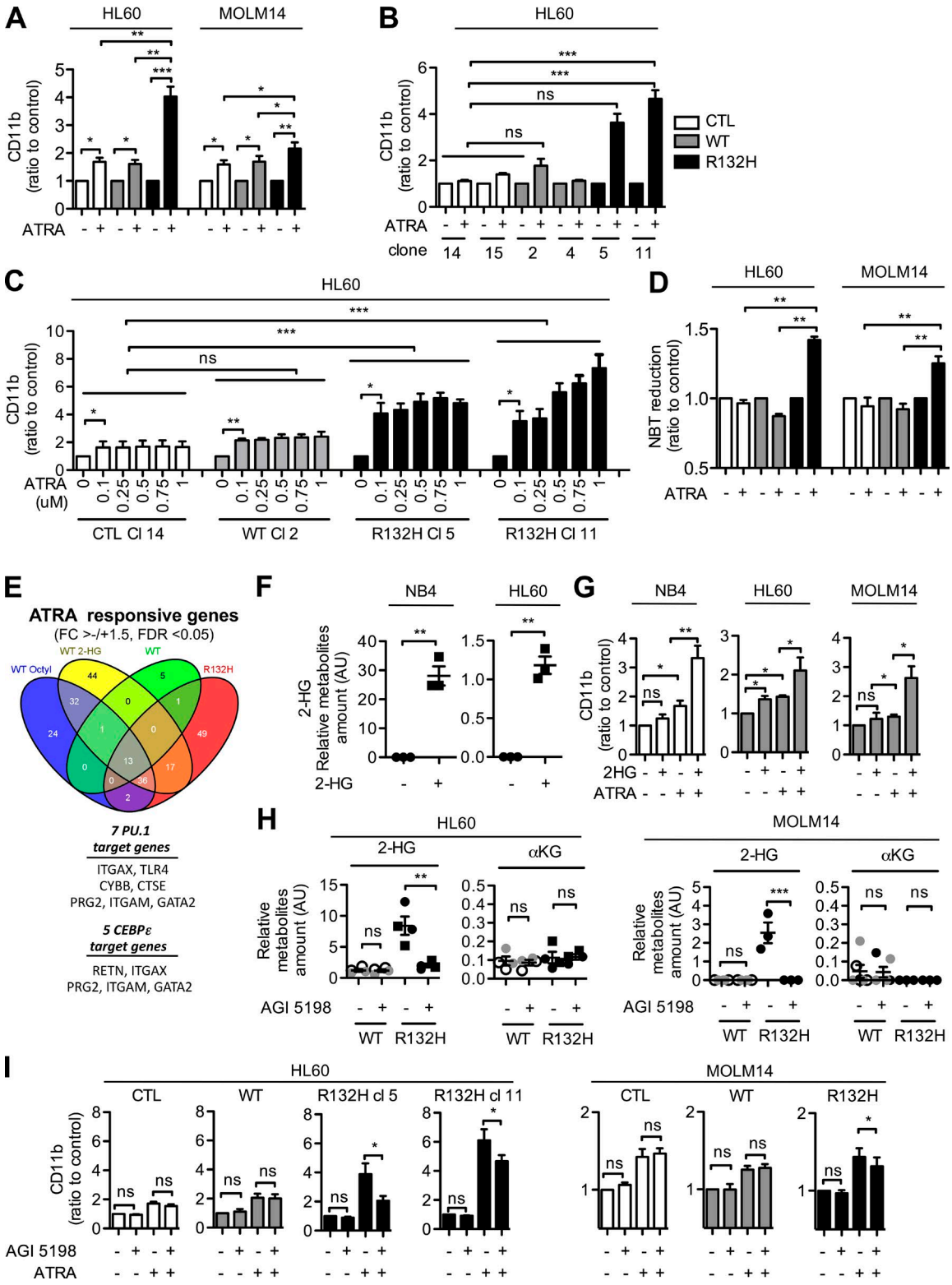

Figure 4. **IDH1–R132H mutation sensitizes to ATRA-induced differentiation of AML cell lines in vitro.** (A–D) Analysis of ATRA-induced differentiation in HL60 and MOLM14 infected with retroviruses encoding GFP alone (CLT) or GFP and the indicated IDH1 variants. (A) Quantification of the CD11b expression measured by flow cytometry after 3-d treatment with 1 µM ATRA or solvent (ratio of mean fluorescence intensity in ATRA-treated to vehicle-treated cells ± SEM; $n = 5$). Mann-Whitney test. (B) Quantification of the CD11b expression measured by flow cytometry after 3-d treatment with 1 µM ATRA or solvent (ratio of mean fluorescence intensity in ATRA-treated to vehicle-treated cells ± SEM; $n = 5$) in different clones (CTL, clones 14–15;

in AML patients (DiNardo et al., 2013; Wang et al., 2013b; Janin et al., 2014). Our observation that 2-HG levels correlate with the ability of ATRA to induce terminal differentiation further support the contention that this therapeutic strategy is likely to be most relevant for the category of AML patients producing highest levels of 2-HG and would be an alternative therapeutic strategy for AML patients developing resistance to mutant IDH inhibitors. It is noteworthy that this therapeutic approach may also be relevant and of benefit for AML patients harboring IDH2 mutations. Because IDH1 mutations are present in preleukemic hematopoietic stem cells and systematically conserved at relapse, this therapeutic strategy holds promise to specifically achieve a long-term remission for this AML patient subgroup.

MATERIALS AND METHODS

AML patient samples. AML and normal bone marrow samples were obtained from patients at the Department of Hematology (Centre Hospitalier Universitaire de Toulouse [CHU], Toulouse, France) after consent in accordance with the Declaration of Helsinki. Samples were stored at the HIMIP collection. In accordance with French law, HIMIP collection has been declared to the Ministry of Higher Education and Research (CD 2008–307 collection 1) and a transfer agreement was obtained (AC 2008–129) after approbation by ethical committees (Comité de Protection des Personnes Sud-ouest et Oustremer II). Clinical and biological annotations of the samples have been declared to the Comité National Informatique et Libertés (i.e., Data Processing and Liberties National Committee). All patients were diagnosed at the Department of Hematology (CHU, Toulouse, France). Their characteristics are summarized in Table S3. Samples containing at least 80% blasts were grown in H4230 methylcellulose medium (STEMCELL Technologies) and ATRA or the control. Primary patient AML cells were plated in 35-mm Petri dishes in duplicate with or without ATRA at 1 μM. After 12-d incubation in a humidified CO_2 incubator, cells were washed three times with PBS at 37°C. If the patient blasts were known to not grow in methyl cellulose medium (assessed routinely at diagnosis in our center), they were co-cultured with human mesenchymal stem cells in IMDM (Life Technologies) supplemented with 15% bovine serum albumin, insulin, and transferrin (STEMCELL Technologies), 100 U/ml of penicillin and streptomycin (Invitrogen), 5 μM β-mercaptoethanol (Invitrogen), 1 mM pyruvate (Sigma-Aldrich), MEM 1X (Sigma-Aldrich), 100 ng/ml DNase (MP Biomedicals), 10 ng/ml hIL3, 100 ng/ml hSCF, and 10 ng/ml human thrombopoietin (all from R&D Systems) at 10^6 cells/ml. All the samples were then processed for treatment with different reagents.

Targeted resequencing. A panel of 31 genes frequently mutated in AML and myeloid malignancies, including *TET2*, *CEBPA*, *DNMT3A*, *IDH1*, and *IDH2*, was designed. Amplicon libraries were obtained from 112 ng DNA per sample, using HaloPlex Target Enrichment System (Agilent Technologies) according to the manufacturer's protocol, with the exception that all volumes of reactions were halved. Sequencing was performed using a MiSeq sequencer (Illumina) following the manufacturer's recommendations. Results were analyzed after alignment of the readings using SureCall Software version 3.0.1.4 (Agilent Technologies). BWA MEM algorithm was used for alignment and SNP PET SNP Caller (Illumina) algorithm was used to identify SNP and INDELs variants. Minimum allele frequency for variant calling was set at 5% with a minimum local depth of 40. All variants were manually checked using IGV version 2.3 software. Complementary detection of described polymorphisms was performed by an in-house software using Ensembl database.

WT clones 4–7; R132H, clones 5–11; Mann-Whitney test). (C) Dose-dependent increase of CD11b expression induced after 3-d treatment with 1 μM ATRA or solvent (ratio of mean fluorescence intensity in ATRA-treated to vehicle-treated cells ± SEM; $n = 5$) in HL60 cells parental, control (Cl 14), WT (Cl 2), or with IDH1–R132H mutations (clone 5 or 11). Two-way ANOVA. (D) Measurement of NBT reduction after 12-d treatment with 1 μM ATRA or control. The data correspond to the mean of three independent experiments (Mann-Whitney test). (E) Venn diagram of the overlapping genes enriched in mutant IDH1 HL60 cells (R132H) versus WT IDH1 HL60 cells both treated with 1 μM ATRA for 24 h with a FDR <0.05, considered as differentially expressed mRNA irrespective of the fold-change. Gene to TF associations specifically within 109 mutant IDH1–R132H target genes in response to ATRA using data mining algorithm (Genomatix). Similar screening and analysis was performed in WT IDH1 HL60 cells with exogenous 2-HG (WT+2-HG) versus WT IDH1 HL60 cells both treated with 1 μM ATRA for 24 h. (F and G) NB4, IDH1–WT HL60 clone, or MOLM14 were treated with or without 100 or 50 μM, respectively, 2-HG for 3 d with 1 μM ATRA or control. (F) Intracellular amounts of 2-HG in parental NB4 cell line or HL60 cell lines expressing WT IDH1 (WT) with or without treatment with 1-octyl-(R)-2-HG determined by LC/MS. The amounts were normalized using a labeled standard, [^{13}C]-succinate, spiked with the same volume in each sample (y axis). Each condition represents a triplicate set of measurements. **, $P < 0.01$; Mann-Whitney test. (G) Quantification of the CD11b expression measured by flow cytometry (ratio of mean fluorescence intensity in ATRA-treated to vehicle-treated cells ± SEM; $n = 5$; Mann-Whitney test). (H and I) Control, WT, or R132H (clone 5 or clone 11) HL60 cells (M) or Control, WT, or R132H MOLM14 cells were pretreated with 2 μM AGI 5198 or solvent for 15 d followed by 3-d treatment for HL60 or 24-h treatment for MOLM14 with or without 1 μM ATRA ± 2 μM AGI 5198 or solvent. Mann-Whitney test. (H) Intracellular amounts of 2-HG and α-KG in HL60 cell lines or MOLM14 cell lines expressing WT IDH1 (WT) or mutant IDH1–R132H (R132H) after or without treatment with IDH1–specific inhibitor AGI-5198 determined by LC/MS (method 2). The amounts were normalized using a labeled standard, [^{13}C]-succinate, spiked with the same volume in each sample (y axis). Each condition represents a triplicate. ** indicates high statistical relevance ($P < 0.01$; Mann-Whitney test). (I) CD11b expression was then measured by flow cytometry (ratio of mean fluorescence intensity in ATRA-treated to vehicle-treated cells ± SEM; $n = 5$). *, $P \leq 0.05$; **, $P \leq 0.01$; and ***, $P \leq 0.001$, statistical significance of the observed differences (Mann-Whitney test).

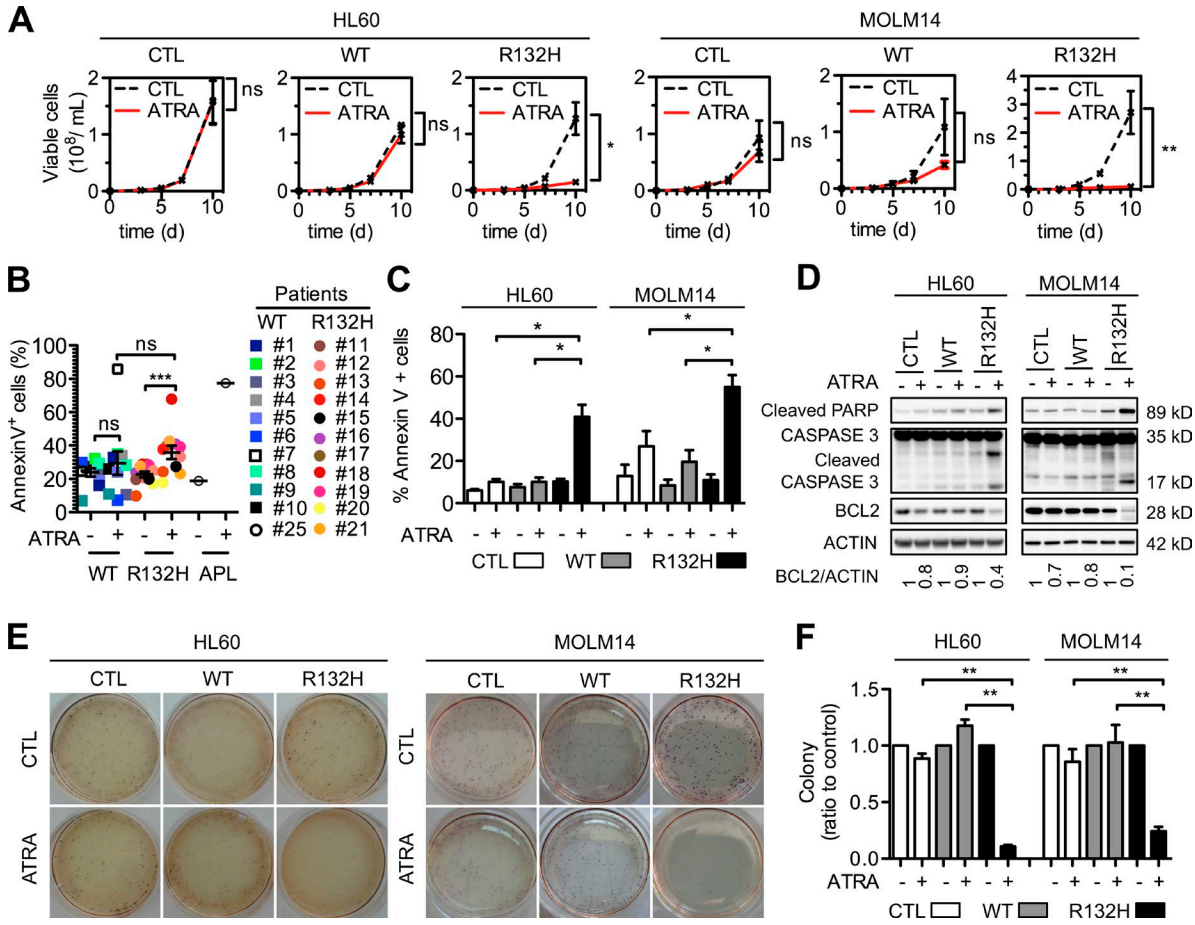

Figure 5. **ATRA preferentially reduces cell viability of mutant IDH1 AML cells through apoptotic cell death in vitro.** (A) HL60 or MOLM14 cell lines expressing GFP alone (CTL) or GFP and the indicated IDH1 variants were cultured with or without 1 µM ATRA for 10 d. Viable cells were counted by Trypan blue dye exclusion ($n = 3$). Two-way ANOVA. (B) ATRA treatment induces granulocytic differentiation of 11 primary patient samples carrying mutant IDH1–R132H (R132) compared with 10 WT IDH1 (WT) and 1 PML-RARα fusion protein (APL). Wilcoxon matched pairs signed rank test. (C) After 5-d treatment with 1 µM ATRA or solvent, the percentage of Annexin V–positive cells was measured by flow cytometry (mean ± SEM, $n = 5$; Mann-Whitney test). (D) HL60 or MOLM14 cells were treated with 1 µM ATRA or solvent for 5 d. BCL2 protein expression and cleavage of poly (ADP-ribose) polymerase or caspase-3 were analyzed by Western blotting. One representative experiment of three experiments is shown. (E and F) HL60 or MOLM14 were plated in methylcellulose in the presence or absence of 1 µM ATRA for 7 d. Representative photographs taken at the end of culture are shown. (F) L-CFU were counted (mean ± SEM; $n = 3$). *, $P \leq 0.05$; **, $P \leq 0.01$; and ***, $P \leq 0.001$, statistical significance of the observed differences (Mann-Whitney test). ns, not significant.

Clonogenic assays. 1,000 AML cells/ml were plated in duplicate in 35-mm Petri dishes in H4230 Stem Cell Technologies methylcellulose medium (STEMCELL Technologies) supplemented with 10% of 5637 cell line–conditioned medium (Dos Santos et al., 2008) and the different reagents. After a 7-d incubation in a humidified CO_2 incubator, 500 µl of MTT at 10 mg/ml was gently added to the methylcellulose and incubated for 2 additional hours at 37°C in a humidified CO_2 incubator. Photographs of dishes were taken and dark purple (viable) colonies were counted.

Generation of mutant IDH1–R132H, WT IDH1–WT, and control (empty) AML cell lines. Human AML cell lines NB4 (DMSZ), HL60 (DMSZ), and MOLM14 cells (Matsuo et al., 1997), provided by M. Carroll (University of Pennsylvania, Philadelphia, PA), were cultured in RPMI-1640 medium (Life Technologies) supplemented with 10% fetal bovine serum (Sigma-Aldrich) and 100 U/ml penicillin and streptomycin (Invitrogen) in an incubator at 37°C and 5% CO_2. HL60 and MOLM14 were transduced with IDH1–R132H, IDH1–WT, or control vector MIGR1 (CTL), as previously described by Figueroa et al. (2010a,b). For MOLM14, bulk preparations were used for all the experiments. For HL60, subclones of (IDH1–R132H, IDH1–WT, or control constructs were generated by sorting GFP-positive cells in each well of a 96-well plate with a FACS Sorter (FACSARIA II SORP; BD). 10 subclones of each group (IDH1–R132H, IDH1–WT, or control) were established. Two clones of each category were then selected for further studies. They were grown

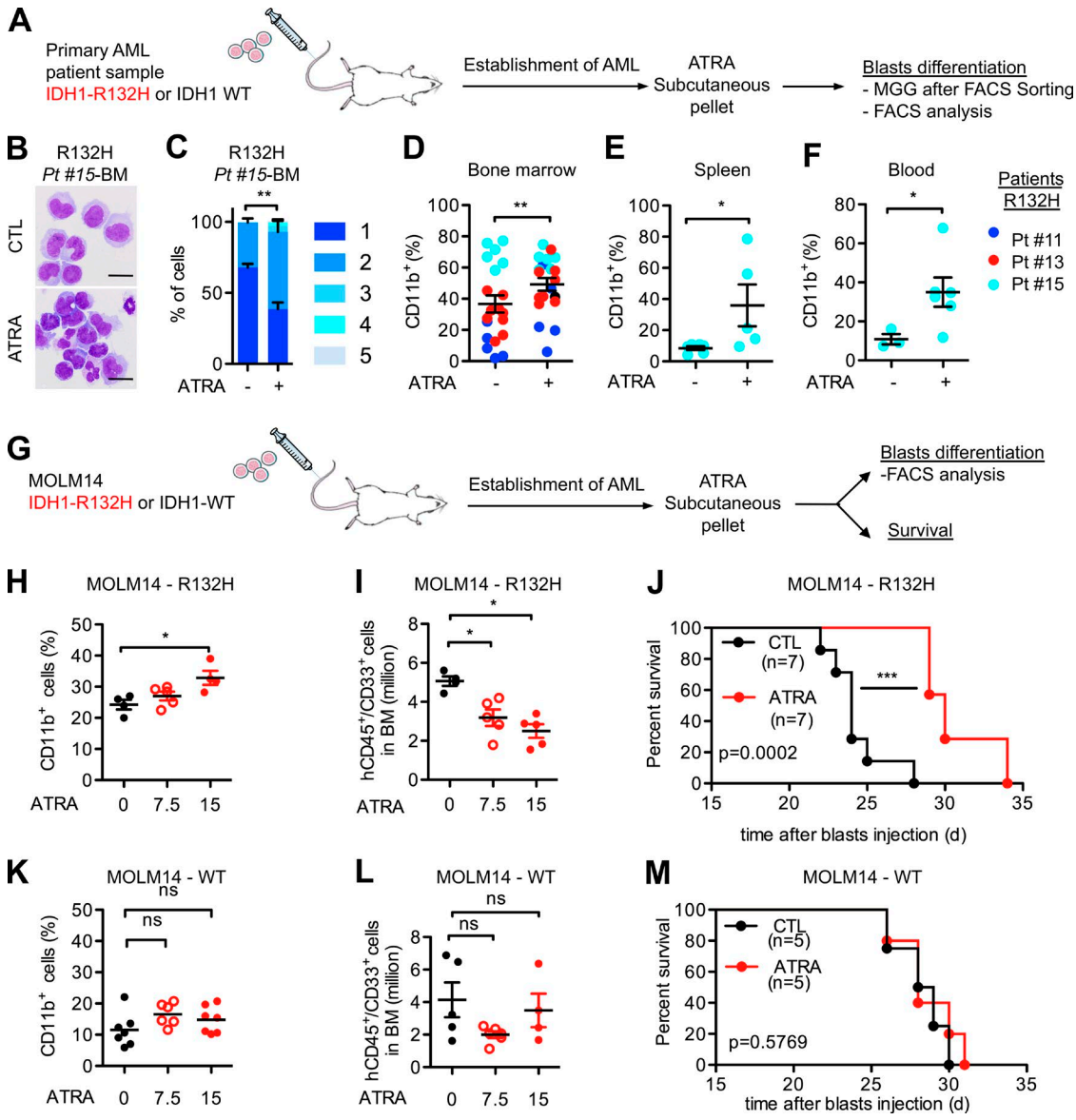

Figure 6. **In vivo antileukemic activity of ATRA in cell line model and primary patient blasts carrying IDH1 R132H mutation.** (A) Schematic representation of the in vivo protocol used for B–F. Immunodeficient NOD-scid IL2rγ^{null} (NSG) female mice were xenografted with IDH1 R132 or WT primary AML patient samples. When AML disease was established, mice were treated with subcutaneous (B–F) ATRA pellet at 2.5 mg (B and C) or 7.5 mg (D–F) pellet or control for 21 d. (B) Human cells were sorted from mice bone marrow, cytospun, and stained with May-Grünwald Giemsa. A representative picture is shown. (C) Cells were classified in 5 categories (from less to more differentiated in accordance of their morphological changes). 100 cells per condition were counted three times (Mann-Whitney test). Percentage of human (hCD45$^+$mCD45$^-$hCD33$^+$hCD44$^+$) CD11b$^+$ cells was measured by flow cytometry analysis in bone marrow (D), spleen (E), and peripheral blood (F) of primary patient samples-xenografted mice. (Patient 1, $n = 5$ untreated and 5 treated mice; patient 2, $n = 6$ untreated and 6 treated mice; patient 3, $n = 9$ untreated and 9 treated mice). (G) Schematic representation of the in vivo protocol used for H–M. (H–M) Immunodeficient NOD-scid IL2rγ^{null} (NSG) female mice were xenografted with MOLM14 transduced with IDH1 R132H (H–J) or WT (K–M). When AML disease was established, mice were treated with subcutaneous ATRA pellet (five mice per group) or control (four mice per group). Blast differentiation and mice overall survival with or without ATRA (7.5 or 15 mg subcutaneous pellet) were monitored in vivo. After 6-d treatment, the percentage of human (hCD45$^+$mCD45$^-$hCD33$^+$hCD44$^+$) CD11b$^+$ cells was assessed by flow cytometry (H and K) and the total cell tumor burden in bone marrow (hCD45$^+$mCD45$^-$hCD33$^+$hCD44$^+$Annexin-V^{neg}) cells was analyzed by flow cytometry in mutant IDH1–R132H (I) or WT (L) IDH1–WT MOLM14-xenografted mice. Mann-Whitney test. Survival of mutant IDH1–R132H (J) or WT (M) IDH1–WT MOLM14-xenografted mice treated with vehicle (CTL, $n = 7$) or ATRA (7.5 mg subcutaneous pellet, $n = 7$). *, $P \leq 0.05$; **, $P \leq 0.01$; and ***, $P \leq 0.001$ indicate statistical significance of the observed differences (Log-rank [Mantel-Cox] test).

<10 passages after resuscitation. All clones were periodically authenticated by morphological inspection and protein expression and tested negative for mycoplasma.

Reagents. ATRA (Sigma-Aldrich) was dissolved in DMSO (max. 1/1,000 final dilution). 1-Octyl ester of (R)-2-HG was synthesized at the Organic Synthesis Core (Memorial Sloane-Kettering Cancer Center, New York, NY) as previously described in Losman et al. (2013) and dissolved in DMSO (max. 1/1,000 final dilution). Octylalcohol (Sigma-Aldrich) solution in DMSO at the same concentration of (R)-2-HG was used as a control solution to assure that only the effect of (R)-2-HG–free acid on the cells was observed. AGI-5198 (EMD Millipore) was dissolved in dimethylfuran (max. 1/1,000 final dilution).

Protein analysis. Western blot analyses were performed as previously described (Lu et al., 2012). Mutant IDH1–R132H and total IDH1 were detected with rabbit monoclonal antibodies to IDH1–R132H (clone H09; 1:1,000; Dianova) and with rabbit monoclonal antibody to IDH1 (clone 2DH1; 1:1,000; Cell Signaling Technology), caspase 3 by rabbit polyclonal antibody (1:1,000; Cell Signaling Technology), Bcl-2 by rabbit polyclonal antibodies (1:1,000; Cell Signaling Technology), and actin by mouse monoclonal antibodies (1:5,000; Santa Cruz Biotechnology, Inc.). Standard secondary antibodies conjugated to HRP were used after incubation with primary antibodies. Immunoreactive bands were visualized by enhanced chemiluminescence (PI32209; Thermo Fisher Scientific) with a Syngene camera.

Extraction of metabolites. Metabolite extraction was performed on frozen pellets (−80°C) of cells. Cell pellets were lysed with a cold (−20°C) mixture of 70% methanol and 30% water, scraped, and vortexed 20 s for a maximal lyse. The samples were centrifuged (18,000 *g*, 4°C, 30 min), and the supernatants were collected. A calculated volume containing the equivalent of 0.5 million cells was dried under nitrogen. Dried extracts were dissolved in 100:40 µl of mobile phase A + 60 µl of mobile phase B.

Intracellular metabolite quantification. Targeted HPLC-MS/MS experiments were performed using an Acquity HPLC system coupled to a triple-quadrupole Xevo TQ MS (Waters Corp.). The software interface was MassLynx (version 4.1). Chromatographic separation was performed on Sequant ZICpHILIC 5 µm, 2.1 × 150 mm at 15°C (Merck). Mobile phase A consisted of an aqueous buffer of 10 mM of ammonium carbonate in water with ammonium hydroxide to adjust basicity to pH 10.5, and mobile phase B of 100% AcN. Chromatographic elution was achieved with a flow rate of 200 µl/min. After injection of 10 µl sample, elution started with an isocratic step of 1 min at 80% B, followed by a linear gradient from 80 to 40% of phase B from 1 to 6 min. The chromatographic system was then rinsed for 5 min at 0% phase B, and the run was ended with an equilibration step of 9 min. The column effluent was directly introduced into the electrospray source of the mass spectrometer, and analyses were performed in the negative ion mode. Source parameters were as follows: droplet evaporation temperature, 350°C; desolvation and cone gas flow rates, (L/h) 650 and 30; capillary voltage, −2.5 kV. Mass resolution parameters LM 1 and HM 1 were fixed at 3 and 15, respectively. MRM transitions were optimized for 2-HG and α-KG detection. For 2-HG, the MRM transition m/z 147 to 129 was monitored with a collision energy of 12 eV and a cone voltage of 15 V. For α-KG the MRM transition m/z 144 to 101 was monitored with a collision energy of 10 eV and a cone voltage of 12 V. MassLynx software was used for peak detection and integration.

Quantitative PCR (qPCR). cDNAs were synthesized from 500 ng total RNA using SuperScript III Reverse transcription (Invitrogen). Real-time qPCRs were performed on a LightCycler 480 SW 1.5 apparatus (Roche) with Platinum Taq DNA polymerase (Invitrogen) and a SYBR green mix containing 3 mM $MgCl_2$ and 30 µM of each dNTP using the following amplification procedure: 45 cycles of 95°C for 4 s, 60°C for 10 s, and 72°C for 15 s. The relative mRNA copy number was calculated using Ct value and was normalized with *Tbp* transcripts. Sequence of primers used for PCR can be provided upon request.

ChIP. Cells (5,106 cells) were trypsinized and counted before cross-link (5 min 1% formaldehyde/1% paraformaldehyde added in the culture medium). Glycine was added at 125 mM final for 5 min to stop the cross-linking. Cells were then rinsed with cold PBS. Cell nuclei were isolated after incubation for 5 min on ice in buffer A (20 mM Hepes, pH 7.8, 10 mM KCl, 0.25% Triton X-100, 1 mM EDTA, and 0.5 mM EGTA, supplemented with protease inhibitors). After centrifugation, nuclei were resuspended in buffer B (10 mM Tris, pH 8.0, 200 mM NaCl, 1 mM EDTA, 0.5 mM EGTA, and protease inhibitors) for 10 min on ice. Nuclei were lysed and chromatin extracted with lysis buffer (10 mM Tris, pH 8.1, 40 mM NaCl, 0.1% SDS, 0.5% Triton X-100, 0.05% NaDoc, 1 mM EDTA, 0.5 mM EGTA, and protease inhibitors) at a final concentration corresponding to 10 million cells/ml. Chromatin sonication was achieved with a sonicator (epishear; Active Motif). MDM2 ChIP was performed by incubating 500 µl (prepared from 5 million cells) of chromatin prepared from H1299 cells with 20 µl of protein G-Dynabeads (Life Technologies) and 5 mg of CEBPα (C-18; Santa Cruz Biotechnology, Inc.) goat polyclonal antibody, or an irrelevant antibody. After overnight incubation, immunoprecipitates were successively washed with five buffers: W1 (10 mM Tris, pH 8.0, 150 mM KCl, NP-40 0.5%, and 1 mM EDTA), W2 (10 mM Tris, pH 8.0, 100 mM NaCl, 0.1% NaDoc, and 0.5% Triton X-100), W3a (10 mM Tris, pH 8.0, 400 mM NaCl, 0.1% NaDoc, and 0.5% Triton X-100), W3b (10 mM Tris, pH 8.0, 500 mM

NaCl, 0.1% NaDoc, and 0.5% Triton X-100), W4 (10 mM Tris, pH 8.0, 250 mM LiCl, 0.5% NaDoc, 0.5% NP-40, and 1 mM EDTA), and W5 (10 mM Tris, pH 8.0, and 1 mM EDTA). Input and immunoprecipitated DNA were decrosslinked overnight at 65°C, diluted in TE, and incubated first with RNaseA (37°C, 45 min), and then with proteinase K (55°C, 45 min). Proteins were removed with phenol-chloroform-isomalylic-alcohol extraction and DNA was recovered by chromatography (nucleospin extract II columns; Macherey-Nagel). For ChIP-qPCR, 1/100 (0.5 µl) of input or immunoprecipitated DNA was analyzed by qPCR with SYBR green (Takara Bio Inc.) on a LightCycler 480 apparatus (Roche). Results are represented as the mean value of at least three independent experiments of immunoprecipitated chromatin (percentage of input) with the indicated antibodies after normalization using a control ChIP performed with an irrelevant antibody. Sequence of primers used for qPCR can be provided upon request.

Gene expression analysis. Total RNAs were extracted from AML clones expressing WT IDH1–WT or mutant IDH1–R132H gene using the QIAGEN kit according to the manufacturer's instructions. RNA purity and integrity were monitored using NanoDrop ND-1000 spectrophotometer and Agilent 2100 Bioanalyzer with RNA 6000 Nano assay kit. Only RNAs with no sign of contamination or marked degradation (RIN > 9) were considered good quality and used for further analysis. Transcriptome profiling assays were performed using the Affymetrix Human Gene GeneChip 2.0 ST arrays. In brief, 250 ng of total RNAs were reverse transcribed into cDNA, and then transcribed into cRNAs and labeled into biotinylated cRNA using the GeneChip WT PLUS Reagent kit (Affymetrix) according to the manufacturer's standard protocols (P/N 4425209 Rev.B 05/2009 and P/N 702808 Rev.6). Labeled cRNA products were randomly fragmented and hybridized onto Affymetrix GeneChips. Upon hybridization, arrays were washed and stained using the Affymetrix GeneChip WT Terminal Labeling and Hybridization kit, before being scanned using a GeneChip Scanner 3000.

Microarray data analysis. CEL files generated after upon array scanning were imported into the Partek Genomics Suite (GS) 6.6 for further analysis. For this purpose, Partek options were set up for GC-content adjustment, robust multiarray background correction, quantile normalization, $\log_2$ transformation, and mean summarization. Data were first preprocessed to estimate transcript cluster expression levels from raw probe signal intensities. Resulting expression data were then imported into R statistical environment for further processing. First, nonspecific filtering was applied to keep only transcript clusters, which belong to the main category. Next, quality of the dataset was assessed through box plots, relative log expressions, and pairwise sample correlations. Principal variance component analysis (PVCA) was also applied to the data. This method estimates the percentage of variability relative to each experimental parameter. As principal variance component analysis revealed a batch effect, the removebatcheffect method of LIMMA package (R/Bioconductor) was used to correct for this effect. Finally, the Rank Product algorithm was used to estimate the statistical significance of the difference in gene expression between different conditions. Genes with pfp <0.05 and absolute fold change ≥1.5 were considered to be differentially expressed.

Data exploration and mining. Lists of DE mRNA (FC > ±1.5 and FDR < 0.05) obtained throughout the study were uploaded in the Genome Analyzer bioinformatics tool (Genomatix) for further functional analyses (GO term, TFs, and small molecules) based on the Genomatix literature mining. The significance of the association between each list and functions or canonical pathways was measured by Fisher's exact test. As a result, a p-value was obtained, determining the probability that the association between the genes in our dataset and a function or canonical pathway can be explained by chance alone. Transcriptional gene regulatory networks were built based on the molecular relationship repertoire referenced in the Genomatix library. The Genomatix Upstream Regulators analytic was also used to identify the transcriptional regulators that could explain the experimental gene expression patterns, predict their activation state, and determine the biological functions affected by the regulatory cascade. We examined the enrichment of our IDH1 mutation gene signature with existing gene expression sets from AML patient specimens with clinicobiological data available under GEO accession no. GSE6891 using GSEA software.

Analysis of granulomonocytic differentiation. We treated cells with ATRA (Sigma-Aldrich) for the indicated time before analysis. We performed FACS analysis of CD11b, CD14, and CD15 expression on 5×10^5 cells using the following anti–human monoclonal antibodies: CD11b-PE (2:100; Beckman Coulter), CD14-AF700 (2:100; BD) for GFP cell lines or CD14-FITC (2:100; BD) for patient samples, CD15-APC (2:100; BD), CD45-APC-H7 (2:100; BD), CD33 BV711 (2:100; BD), and CD44 PeCy7 (2:100; BD) after washing with PBS. Antimurine antibody CD45-PerCP Cy5.5 was added for in vivo analysis. Flow cytometry analysis was performed using a Fortessa flow cytometer (BD), and data were analyzed with FlowJo software. A minimum of 10,000 events was collected. Apoptotic cells were stained with Annexin V-PB according to the manufacturer's protocol (BD). We analyzed the level of the NBT reducing activity after differentiation using the method of Sakashita et al. (1991) with a slight modification. Treated or control cells were resuspended in phorbol-12-myristate-13-acetate (PMA) to a final concentration of 200 ng/ml. 20 µl of MTS was added in 200 µl of cell suspension control or treated. After a 2-h incubation at 37°C and 5% CO_2 in an incubator, the amount of formazan formed was assayed spectrophotometrically at 570 nm. For the morphological analysis of myeloid cell differentiation, we prepared cytospins by centrifugation in 150 µl PBS at a speed of 300 rpm for 5 min using Superfrost

Plus positively charged glass slides. We stained cytospun slides at room temperature with May-Grünwald Giemsa (Sigma-Aldrich). 100 cells were counted in triplicate for each condition and examined for cellular morphology using an Axioskop microscope with AxiCam camera (Carl Zeiss).

In vivo treatment of AML in NSG mice. Female NSG mice were produced at the UMS006 in Toulouse (France) using breeders obtained from Charles River. NSG mice were bred and housed at the Purpan Hospital. All animal experimental protocols were approved by the institutional Animal Care and Use Ethical Committee of the UMS006 and Région Midi-Pyrénées (approval #13-U1037-JES08). NSG mice were treated by an i.p. injection of busulfan (20 mg/kg) before i.v. xenotransplantation of AML. All the mice in the same experiment received equal numbers of cells (2×10^6 cells for MOLM14-IDH1WT or IDH1R132H or 10^6 primary patient specimens), and then a daily monitoring of mice for symptoms of disease (ruffled coat, hunched back, weakness, and reduced motility). At the disease establishment (after flow cytometric analysis of bone marrow aspirate or blood sample identifying human blasts), ATRA was administrated to xenografted mice by subcutaneous implantation of a 21-d release 2.5- or 7.5-mg ATRA pellet (Innovative Research of America). After 6 d (for xenografted mice with cell lines) or 21 d (for xenografted mice with primary AML patient sample) ATRA treatment, mice were humanely sacrificed to analyze bone marrow engraftment. For xenografted mice with cell lines, a second group of mice was used to follow overall mouse survival. Bone marrow (mixed from tibias and femurs) were crushed into HBSS with 1% SVF, washed in PBS, and dissociated into single-cell suspensions for analysis by flow cytometry of human leukemic cell engraftment and bone marrow cell tumor burden. $CD33^+CD44^+$ $hCD45^+mCD45^-AnnexinV^-$ cells were assessed by flow cytometry, and the differentiation of human cells was assessed with CD11b, CD15, and CD14 markers. For the morphological analysis of myeloid differentiation, 150,000 human blasts ($CD33^+CD44^+hCD45^+mCD45^-AnnexinV^-$ cells) were sorted with a FACS Sorter (FACSARIA II SORT; BD), cytospun, and stained with May-Grünwald Giemsa staining.

Statistical analyses. The Kaplan-Meier method was used to estimate the leukemia-free survival in xenografted mice. Log-rank p-values were used for comparisons of the leukemia-free survival among three subgroups. The other statistical analyses were performed using the Mann-Whitney U-Test using the Prism software package (GraphPad Software). Results are expressed as mean ± SEM. Differences were considered as significant for p-values <0.05. *, $P < 0.05$; **, $P < 0.01$; ***, $P < 0.001$.

Online supplemental material. Fig. S1 shows the validation of a specific gene signature in AML cells with IDH1–R132H mutation. Table S1 shows the list of up- and down-regulated genes in mutant IDH1–R132H AML cells compared with WT IDH1 cells. Table S2 shows the list of co-cited TFs mutant IDH1–R132H AML cells compared with WT IDH1 cells. Table S3 shows the clinical characteristics of 25 AML patients bearing or lacking an IDH1–R132 mutation. Table S4 shows the list of differentially expressed genes in mutant IDH1–R132H AML cells compared with WT IDH1 cells after ATRA treatment. Table S5 lists ATRA-responsive genes. Online supplemental material is available at http://www.jem.org/cgi/content/full/jem.20150736/DC1.

ACKNOWLEDGMENTS

We thank Mr. Xinxu Shi for assisting with synthesis, Dr. George Sukenick and Ms. Joan Subrath from the NMR Analytical Core Facility for help with NMR and LC/MS Spectra. MetaToul (Metabolomics and Fluxomics Facilities, Toulouse, France) is gratefully acknowledged for carrying out metabolome analysis. MetaToul and LEMM are part of the national infrastructure MetaboHUB-ANR-11-INBS-0010 (The French National infrastructure for metabolomics and fluxomics). The authors also thank G. Bossis, M. Piechaczyk, E. Duprez, V. Penard-Lacronique, M.A. Selak, and M. Carroll for critical reading of the manuscript. The authors would like to thank the members of the Team 8 and 18, of the animal and flow cytometry core facilities, A. Sarry, A.-M. Bénot, and R. Tang.

This work was supported by grants from the French government under the program "Investissement d'avenir" Cancer Pharmacology of Toulouse-Oncopole and Region (ANR-11-PHUC-001) and the project METAML (INCA-2012-105), from the Fondation Innabiosante/Toulouse Cancer Santé, the Fondation ARC, the Association Laurette Fugain under the program RESISTAML, and the Association G.A.E.L. H. Boutzen was supported by the Fondation pour la Recherche Médicale (FDT20140930983). F. de Toni had a fellowship from the Fondation de FranceWork at the Organic Synthesis Core is partially funded through National Cancer Institute Core grant P30 CA008748-48. MetaToul is supported by grants from the Région Midi-Pyrénées, the European Regional Development Fund, the SICOVAL, the Infrastructures en Biologie Sante et Agronomie (France), the Centre National de la Recherche Scientifique (CNRS), and the Institut National de la Recherche Agronomique (INRA).

The authors declare no competing financial interests.

Author contributions: H. Boutzen, C. Récher, and J.E. Sarry designed the studies, interpreted the data, and wrote the manuscript; H. Boutzen performed the experiments; L. Gales and F.A. Castelli performed 2-HG and metabolomic experiments; G. Yang and O. Ouerfelli synthesized the cell permeable 2-HG; L. Vallar and T. Kaoma performed transcriptomic analyses; V. Mansat-de Mas, and E. Delabesse managed the tissue biobank and performed mutational analyses; P. Hirsch and F. Delhommeau contributed to NGS design and analysis; E. Saland, C. Larrue, M. David, and F. de Toni contributed to the in vivo experiments. F. Vergez, L. Le Cam, L.K. Linares, L. Stuani, J.C. Portais, and C. Junot assisted with data interpretation.

Submitted: 28 April 2015
Accepted: 2 February 2016

REFERENCES

Abbas, S., S. Lugthart, F.G. Kavelaars, A. Schelen, J.E. Koenders, A. Zeilemaker, W.J. van Putten, A.W. Rijneveld, B. Löwenberg, and P.J. Valk. 2010. Acquired mutations in the genes encoding IDH1 and IDH2 both are recurrent aberrations in acute myeloid leukemia: prevalence and prognostic value. *Blood*. 116:2122–2126. http://dx.doi.org/10.1182/blood-2009-11-250878

Altucci, L., A. Rossin, O. Hirsch, A. Nebbioso, D. Vitoux, E. Wilhelm, F. Guidez, M. De Simone, E.M. Schiavone, D. Grimwade, et al. 2005. Rexinoid-triggered differentiation and tumor-selective apoptosis of acute myeloid leukemia by protein kinase A-mediated desubordination of retinoid X receptor. *Cancer Res.* 65:8754–8765. http://dx.doi.org/10.1158/0008-5472.CAN-04-3569

Bagger, F.O., N. Rapin, K. Theilgaard-Mönch, B. Kaczkowski, L.A. Thoren, J. Jendholm, O. Winther, and B.T. Porse. 2013. HemaExplorer: a database of mRNA expression profiles in normal and malignant haematopoiesis. *Nucleic Acids Res.* 41(D1):D1034–D1039. http://dx.doi.org/10.1093/nar/gks1021

Burnett, A.K., R.K. Hills, C. Green, S. Jenkinson, K. Koo, Y. Patel, C. Guy, A. Gilkes, D.W. Milligan, A.H. Goldstone, et al. 2010. The impact on outcome of the addition of all-trans retinoic acid to intensive chemotherapy in younger patients with nonacute promyelocytic acute myeloid leukemia: overall results and results in genotypic subgroups defined by mutations in NPM1, FLT3, and CEBPA. *Blood*. 115:948–956. http://dx.doi.org/10.1182/blood-2009-08-236588

Chan, S.M., D. Thomas, M.R. Corces-Zimmerman, S. Xavy, S. Rastogi, W.J. Hong, F. Zhao, B.C. Medeiros, D.A. Tyvoll, and R. Majeti. 2015. Isocitrate dehydrogenase 1 and 2 mutations induce BCL-2 dependence in acute myeloid leukemia. *Nat. Med.* 21:178–184. http://dx.doi.org/10.1038/nm.3788

Chelbi-Alix, M.K., and L. Pelicano. 1999. Retinoic acid and interferon signaling cross talk in normal and RA-resistant APL cells. *Leukemia*. 13:1167–1174. http://dx.doi.org/10.1038/sj.leu.2401469

Chou, A.P., R. Chowdhury, S. Li, W. Chen, A.J. Kim, D.E. Piccioni, J.M. Selfridge, R.R. Mody, S. Chang, S. Lalezari, et al. 2012. Identification of retinol binding protein 1 promoter hypermethylation in isocitrate dehydrogenase 1 and 2 mutant gliomas. *J. Natl. Cancer Inst.* 104:1458–1469. http://dx.doi.org/10.1093/jnci/djs357

Dang, L., D.W. White, S. Gross, B.D. Bennett, M.A. Bittinger, E.M. Driggers, V.R. Fantin, H.G. Jang, S. Jin, M.C. Keenan, et al. 2009. Cancer-associated IDH1 mutations produce 2-hydroxyglutarate. *Nature.* 462:739–744. http://dx.doi.org/10.1038/nature08617

DiNardo, C.D., K.J. Propert, A.W. Loren, E. Paietta, Z. Sun, R.L. Levine, K.S. Straley, K. Yen, J.P. Patel, S. Agresta, et al. 2013. Serum 2-hydroxyglutarate levels predict isocitrate dehydrogenase mutations and clinical outcome in acute myeloid leukemia. *Blood*. 121:4917–4924. http://dx.doi.org/10.1182/blood-2013-03-493197

Dos Santos, C., C. Demur, V. Bardet, N. Prade-Houdellier, B. Payrastre, and C. Récher. 2008. A critical role for Lyn in acute myeloid leukemia. *Blood*. 111:2269–2279. http://dx.doi.org/10.1182/blood-2007-04-082099

Fathi, A.T., H. Sadrzadeh, A.H. Comander, M.J. Higgins, A. Bardia, A. Perry, M. Burke, R. Silver, C.R. Matulis, K.S. Straley, et al. 2014. Isocitrate dehydrogenase 1 (IDH1) mutation in breast adenocarcinoma is associated with elevated levels of serum and urine 2-hydroxyglutarate. *Oncologist*. 19:602–607. http://dx.doi.org/10.1634/theoncologist.2013-0417

Ferrari-Amorotti, G., K. Keeshan, M. Zattoni, C. Guerzoni, G. Iotti, S. Cattelani, N.J. Donato, and B. Calabretta. 2006. Leukemogenesis induced by wild-type and STI571-resistant BCR/ABL is potently suppressed by C/EBPα. *Blood*. 108:1353–1362. http://dx.doi.org/10.1182/blood-2006-01-011833

Figueroa, M.E., O. Abdel-Wahab, C. Lu, P.S. Ward, J. Patel, A. Shih, Y. Li, N. Bhagwat, A. Vasanthakumar, H.F. Fernandez, et al. 2010a. Leukemic IDH1 and IDH2 mutations result in a hypermethylation phenotype, disrupt TET2 function, and impair hematopoietic differentiation. *Cancer Cell*. 18:553–567. http://dx.doi.org/10.1016/j.ccr.2010.11.015

Figueroa, M.E., S. Lugthart, Y. Li, C. Erpelinck-Verschueren, X. Deng, P.J. Christos, E. Schifano, J. Booth, W. van Putten, L. Skrabanek, et al. 2010b. DNA methylation signatures identify biologically distinct subtypes in acute myeloid leukemia. *Cancer Cell*. 17:13–27. http://dx.doi.org/10.1016/j.ccr.2009.11.020

Green, C.L., C.M. Evans, L. Zhao, R.K. Hills, A.K. Burnett, D.C. Linch, and R.E. Gale. 2011. The prognostic significance of IDH2 mutations in AML depends on the location of the mutation. *Blood*. 118:409–412. http://dx.doi.org/10.1182/blood-2010-12-322479

Guilhamon, P., M. Eskandarpour, D. Halai, G.A. Wilson, A. Feber, A.E. Teschendorff, V. Gomez, A. Hergovich, R. Tirabosco, M. Fernanda Amary, et al. 2013. Meta-analysis of IDH-mutant cancers identifies EBF1 as an interaction partner for TET2. *Nat. Commun.* 4:2166. http://dx.doi.org/10.1038/ncomms3166

Hasemann, M.S., F.K. Lauridsen, J. Waage, J.S. Jakobsen, A.K. Frank, M.B. Schuster, N. Rapin, F.O. Bagger, P.S. Hoppe, T. Schroeder, and B.T. Porse. 2014. C/EBPα is required for long-term self-renewal and lineage priming of hematopoietic stem cells and for the maintenance of epigenetic configurations in multipotent progenitors. *PLoS Genet.* 10:e1004079. http://dx.doi.org/10.1371/journal.pgen.1004079

Janin, M., E. Mylonas, V. Saada, J.B. Micol, A. Renneville, C. Quivoron, S. Koscielny, L. Scourzic, S. Forget, C. Pautas, et al. 2014. Serum 2-hydroxyglutarate production in IDH1- and IDH2-mutated de novo acute myeloid leukemia: a study by the Acute Leukemia French Association group. *J. Clin. Oncol.* 32:297–305. http://dx.doi.org/10.1200/JCO.2013.50.2047

Kats, L.M., M. Reschke, R. Taulli, O. Pozdnyakova, K. Burgess, P. Bhargava, K. Straley, R. Karnik, A. Meissner, D. Small, et al. 2014. Proto-oncogenic role of mutant IDH2 in leukemia initiation and maintenance. *Cell Stem Cell*. 14:329–341. http://dx.doi.org/10.1016/j.stem.2013.12.016

Kernytsky, A., F. Wang, E. Hansen, S. Schalm, K. Straley, C. Gliser, H. Yang, J. Travins, S. Murray, M. Dorsch, et al. 2015. IDH2 mutation-induced histone and DNA hypermethylation is progressively reversed by small-molecule inhibition. *Blood*. 125:296–303. http://dx.doi.org/10.1182/blood-2013-10-533604

Laiosa, C.V., M. Stadtfeld, and T. Graf. 2006. Determinants of lymphoid-myeloid lineage diversification. *Annu. Rev. Immunol.* 24:705–738. http://dx.doi.org/10.1146/annurev.immunol.24.021605.090742

Losman, J.A., R.E. Looper, P. Koivunen, S. Lee, R.K. Schneider, C. McMahon, G.S. Cowley, D.E. Root, B.L. Ebert, and W.G. Kaelin Jr. 2013. (*R*)-2-hydroxyglutarate is sufficient to promote leukemogenesis and its effects are reversible. *Science.* 339:1621–1625. http://dx.doi.org/10.1126/science.1231677

Lu, C., P.S. Ward, G.S. Kapoor, D. Rohle, S. Turcan, O. Abdel-Wahab, C.R. Edwards, R. Khanin, M.E. Figueroa, A. Melnick, et al. 2012. IDH mutation impairs histone demethylation and results in a block to cell differentiation. *Nature.* 483:474–478. http://dx.doi.org/10.1038/nature10860

Mardis, E.R., L. Ding, D.J. Dooling, D.E. Larson, M.D. McLellan, K. Chen, D.C. Koboldt, R.S. Fulton, K.D. Delehaunty, S.D. McGrath, et al. 2009. Recurring mutations found by sequencing an acute myeloid leukemia genome. *N. Engl. J. Med.* 361:1058–1066. http://dx.doi.org/10.1056/NEJMoa0903840

Matsuo, Y., R.A. MacLeod, C.C. Uphoff, H.G. Drexler, C. Nishizaki, Y. Katayama, G. Kimura, N. Fujii, E. Omoto, M. Harada, and K. Orita. 1997. Two acute monocytic leukemia (AML-M5a) cell lines (MOLM-13 and MOLM-14) with interclonal phenotypic heterogeneity showing MLL-AF9 fusion resulting from an occult chromosome insertion, ins(11;9)(q23;p22p23). *Leukemia*. 11:1469–1477. http://dx.doi.org/10.1038/sj.leu.2400768

Nazha, A., C. Bueso-Ramos, E. Estey, S. Faderl, S. O'Brien, M.H. Fernandez, M. Nguyen, C. Koller, E. Freireich, M. Beran, et al. 2013. The Addition of All-Trans Retinoic Acid to Chemotherapy May Not Improve the Outcome of Patient with NPM1 Mutated Acute Myeloid Leukemia. *Front. Oncol.* 3:218. http://dx.doi.org/10.3389/fonc.2013.00218

Radomska, H.S., C.S. Huettner, P. Zhang, T. Cheng, D.T. Scadden, and D.G. Tenen. 1998. CCAAT/enhancer binding protein α is a regulatory switch sufficient for induction of granulocytic development from bipotential myeloid progenitors. *Mol. Cell. Biol.* 18:4301–4314. http://dx.doi.org/10.1128/MCB.18.7.4301

Sakashita, A., T. Nakamaki, N. Tsuruoka, Y. Honma, and M. Hozumi. 1991. Granulocyte colony-stimulating factor, not granulocyte-macrophage colony-stimulating factor, co-operates with retinoic acid on the induction of functional N-formyl-methionyl-phenylalanine receptors in HL-60 cells. *Leukemia*. 5:26–31.

Sasaki, M., C.B. Knobbe, J.C. Munger, E.F. Lind, D. Brenner, A. Brüstle, I.S. Harris, R. Holmes, A. Wakeham, J. Haight, et al. 2012. IDH1(R132H) mutation increases murine haematopoietic progenitors and alters epigenetics. *Nature.* 488:656–659. http://dx.doi.org/10.1038/nature11323

Schepers, H., A.T. Wierenga, D. van Gosliga, B.J. Eggen, E. Vellenga, and J.J. Schuringa. 2007. Reintroduction of C/EBPα in leukemic $CD34^+$ stem/progenitor cells impairs self-renewal and partially restores myelopoiesis. *Blood*. 110:1317–1325. http://dx.doi.org/10.1182/blood-2006-10-052175

Schlenk, R.F., K. Döhner, M. Kneba, K. Götze, F. Hartmann, F. Del Valle, H. Kirchen, E. Koller, J.T. Fischer, L. Bullinger, et al. German-Austrian AML Study Group (AMLSG). 2009. Gene mutations and response to treatment with all-trans retinoic acid in elderly patients with acute myeloid leukemia. Results from the AMLSG Trial AML HD98B. *Haematologica*. 94:54–60. http://dx.doi.org/10.3324/haematol.13378

Shen, M., R.P. Bunaciu, J. Congleton, H.A. Jensen, L.G. Sayam, J.D. Varner, and A. Yen. 2011. Interferon regulatory factor-1 binds c-Cbl, enhances mitogen activated protein kinase signaling and promotes retinoic acid-induced differentiation of HL-60 human myelo-monoblastic leukemia cells. *Leuk. Lymphoma*. 52:2372–2379. http://dx.doi.org/10.3109/10428194.2011.603449

Shlush, L.I., S. Zandi, A. Mitchell, W.C. Chen, J.M. Brandwein, V. Gupta, J.A. Kennedy, A.D. Schimmer, A.C. Schuh, K.W. Yee, et al. HALT Pan-Leukemia Gene Panel Consortium. 2014. Identification of pre-leukaemic haematopoietic stem cells in acute leukaemia. *Nature*. 506:328–333. http://dx.doi.org/10.1038/nature13038

Turcan, S., D. Rohle, A. Goenka, L.A. Walsh, F. Fang, E. Yilmaz, C. Campos, A.W. Fabius, C. Lu, P.S. Ward, et al. 2012. IDH1 mutation is sufficient to establish the glioma hypermethylator phenotype. *Nature*. 483:479–483. http://dx.doi.org/10.1038/nature10866

Verhaak, R.G., B.J. Wouters, C.A. Erpelinck, S. Abbas, H.B. Beverloo, S. Lugthart, B. Löwenberg, R. Delwel, and P.J. Valk. 2009. Prediction of molecular subtypes in acute myeloid leukemia based on gene expression profiling. *Haematologica*. 94:131–134. http://dx.doi.org/10.3324/haematol.1329918838472

Wang, F., J. Travins, B. DeLaBarre, V. Penard-Lacronique, S. Schalm, E. Hansen, K. Straley, A. Kernytsky, W. Liu, C. Gliser, et al. 2013a. Targeted inhibition of mutant IDH2 in leukemia cells induces cellular differentiation. *Science*. 340:622–626. http://dx.doi.org/10.1126/science.1234769

Wang, J.H., W.L. Chen, J.M. Li, S.F. Wu, T.L. Chen, Y.M. Zhu, W.N. Zhang, Y. Li, Y.P. Qiu, A.H. Zhao, et al. 2013b. Prognostic significance of 2-hydroxyglutarate levels in acute myeloid leukemia in China. *Proc. Natl. Acad. Sci. USA*. 110:17017–17022. http://dx.doi.org/10.1073/pnas.1315558110